Review

Solid State Mechanochemical Processes for Better Electroceramics

Mamoru Senna*

Faculty of Science and Technology, Keio University

** Corresponding author: E-mail: senna@applc.keio.ac.jp*

Received: 23-09-2013

Dedicated to the memory of Prof. Marija Kosec.

Abstract

The present short overview focuses on the renovation of solid state processes toward phase pure and well-crystallized complex oxides centered on the electroceramic materials. Elevation of the reactivity and preservation of stoichiometry of the starting mixture or precursor are of universal importance. Mechanical activation, being considered as versatile, may also need reconsideration in view of contamination and process rationalization. After briefly reviewing mechanochemical processes for direct synthesis of complex oxides, solid state processes toward well crystallized fine particles of complex oxides are discussed by starting from mechanochemically derived precursors with subsequent optimized calcination. Case studies were cited from literatures for complex oxides, including author's own experimental studies mainly with $BaBi_2Ta_2O_9$ (BBT), $Ba(Mg_{1/3}Ta_{2/3})O_3$ (BMT) and $KNbO_3$ (KN). The substances discussed are mostly associated with ferroelectric materials, with a few exceptions of iron-containing magnetic materials.

Keywords: Electroceramics, Precursor, Solid-state reaction, Mechanochemistry, Complex oxide

1. Introduction

Being in the era of increasing energy and cost consciousness of materials production, much effort is paid to fabricate functional complex oxides via environmentally more benign processes.[1–5] A conventional solid state ceramic process, on the other hand, is more advantageous than competing alternatives via solution or vapor phases, due primarily to high productivity, affordability and scalability. To overcome well known shortcomings of inhomogeneity, low reactivity and associated necessity of high temperature, we need to start from better dispersed and more homogeneous reaction mixture. Appropriate choice of the starting species of cationic ingredients may not be underestimated either.

It is quite common to use ball mills to obtain a homogeneous powder mixture. Related to the demands for nanoparticles, various mills appeared to give highest possible energy density. Indeed, mechanochemical synthesis, often coined as mechanosynthesis, became common to obtain the end product simply by co-milling appropriate stoichiometric powder mixture. The process is well established, not only in the genre of metallic alloys, but also complicated oxide systems.[6] However, this does not always match the present purpose from the viewpoints of crystallinity and particle size distribution. High intensity milling is quite often hazardous, due chiefly to serious contamination and stoichiometry loss. In such cases, it is important to exert mechanical stress as sparingly as possible by controlling what is absolutely beneficial by virtue of mechanical stressing, and combining with subsequent thermal processes. Importance and charm of the mechanical stressing under these concepts are recognized and coined as soft-mechanochemical processing.[7–8]

With further demanding requirements from the viewpoints of microelectronics, it is further needed to obtain well-crystallized, and yet fine particulate materials. For this purpose, simple mechanical activation of the starting materials is not always adequate, since it often ends up with undesirable grain growth. To fulfill those demands, we have to think about larger number of nucleation sites and shorter diffusion paths for the crystal growth upon heating the homogeneous precursors, as we have discussed in the case of $BaTiO_3$.[17–19]

The objectives of the present short review are to elucidate the mechanochemical processes needed to obtain

complex oxides, to adapt the requirements mentioned above. For this purpose, the review will start from some representative mechanochemical synthesis processes by citing several representative studies. Subsequently, the principles and examples of soft-mechanochemical processes are discusses, based mainly on the author's own experimental studies. The compounds cited in the case studies are mostly related to the ferroelectric materials, with a few exceptions of iron-containing magnetic materials.

2. Mechanochemical Syntheses of Complex Oxides

Rojac et al. paid efforts to describe the conditions for the mechanochemical synthesis of perovskites by correlating the ball-impact energy with the weight-normalized cumulative kinetic energy released in the system.[20] They further studied the mechanochemical reactions between Na_2CO_3 and transition-metal oxides (V_2O_5, Nb_2O_5 and Ta_2O_5), to elucidate the reaction mechanisms including the formation of amorphous carbonato complex, followed by their decomposition and the crystallization of the final perovskite.[21]

More complicated, multi-component perovskite, $(K,Na,Li)(Nb,Ta)O_3$, KNLNT, was also prepared by mechanochemical synthesis,[22] where they examined the effects of stress components, i.e. impact and impact + friction. As shown in the Fourier transform infrared (FTIR) spectra in Figure 1, the characteristic splitting of the n_3 and the appearance of the n_1 vibration, an indication of the carbonato complex formation, was observed by the milling regime of "impact + friction". In contrast, pure "friction" did not result in the splitting. It is therefore obvious that the "impact" stress component is indispensable for the mechanochemical synthesis of KNLNT.[23] As they calcined the 10 h activated mixture at 800 °C and subsequently sintered in air at 1080 °C for 2 h, they obtained a homogeneously sintered body of KNLNT ceramics.[22]

Stojanovic et al. synthesized single phase $BaTiO_3$ from mixed oxides comprising BaO and TiO_2.[24] They attributed their success in the mechanochemical synthesis to the nucleation of nanocrystallites and subsequent growth of a highly activated oxide matrix. Lazarević et al. succeeded in the mechanochemical synthesis of $Bi_4Ti_3O_{12}$ by co-milling a mixture of Bi_2O_3 and TiO_2.[25] They observed the fine structure of the product, in which $Bi_4Ti_3O_{12}$ (BIT) crystallites were embedded in an amorphous phase of bismuth titanate. They extended the mechanochemical synthesis to the bi-layered structured ferroelectric materials, i.e. BIT and barium-bismuth titanate, $BaBi_4Ti_4O_{15}$ (BBT).[26]

Sepelak et al. prepared nanostructured fayalite (α-Fe_2SiO_4) with a large volume fraction of interfaces via single-step mechanochemical synthesis from a mixture of 2α-Fe_2O_3 + 2Fe + $3SiO_2$.[27] The non-equilibrium state of the as-prepared silicate was characterized by the presence

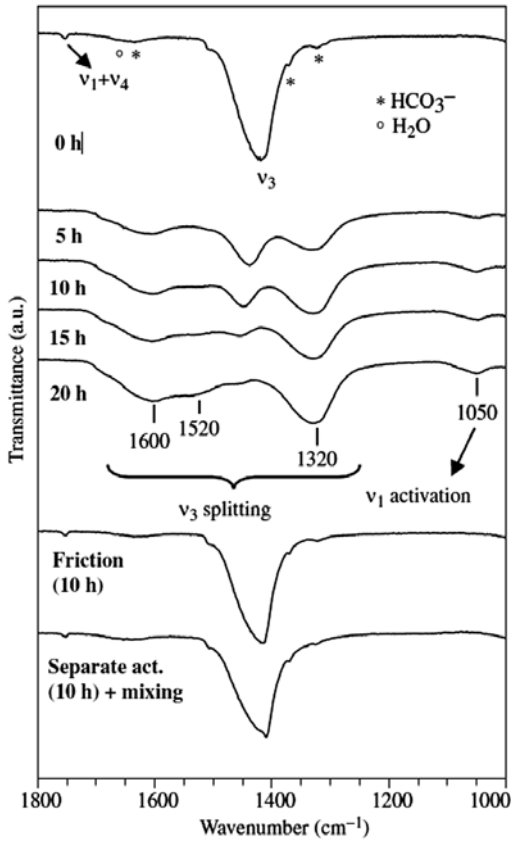

Figure 1. Infrared (IR) spectra of non-activated mixture (0 h) and after activation in the žžimpact1friction'' milling regime for 5, 10, 15, and 20 h. The spectra of the mixture prepared by activation in the žžfriction'' milling regime and by activating the initial powders separately are also shown. Note that n_1, n_3, and n_4 denote CO_3^{2-} vibrations.[22] Reproduced by permission of American Ceramic Society.

of deformed polyhedra in the interface/surface regions of nanoparticles. The ^{57}Fe Mössbauer sextets, corresponding to α-Fe_2O_3 and Fe, collapsed and were gradually replaced by a central doublet characteristic of Fe^{2+} ions.[27] It indicates that the milling generates a complex series of heterogeneous solid-state formation, by the scheme, 2α-Fe_2O_3 +2Fe + $3SiO_2$ = $3Fe_2SiO_4$, which are completed after 4 h.

By the same token, they synthesized nanostructured bismuth ferrite ($BiFeO_3$) via a mechanochemical route from a mixture, α-Fe_2O_3 / Bi_2O_3.[28] ^{57}Fe Mössbauer spectroscopy, together with high-resolution transmission electron microscopy (TEM) and X-ray diffractometry (XRD), revealed a non-uniform structure of mechanochemically synthesized $BiFeO_3$ nanoparticles, consisting of a crystalline core surrounded by an amorphous surface shell. As a consequence of canted spins in the surface shell of nanoparticles, the mechanically synthesized $BiFeO_3$ exhibits an enhanced magnetization, an enhanced coercivity, and a shifted hysteresis loop.

Mechanochemical synthesis is in most cases facile, solvent free and often times very quick.[29] However, the process is not always free from contamination.[30,31] The

problem is suppressed when the milling media are coated by the reacting powders.[32]

3. Concept of Soft-Mechanochemical Synthesis

Concept of a soft-mechanochemical process is based on the bridging bond formation across the grain boundary of the dissimilar oxide or hydroxide particles.[7] Mechanisms of such bridging are two-fold, i.e. an acid-base principle[8,9] and a radical recombination.[10] Bridging bond formation between a typical acidic oxide, SiO_2 with surface silanol groups and a typical basic hydroxide, $Ca(OH)_2$, was demonstrated by ^{29}Si cross-polarization (CP)/ magic angle spinning (MAS) nuclear magnetic resonance (NMR) spectra,[11] which preferentially demonstrate the states of silicon atoms near surface silanolic proton. As shown in Figure 2, the Q_3 peak for silanol groups of pure silica is predominant in a mixture without milling. The Q_4 peak for a standard SiO_4 unit was completely missing. This implies that most of the silicon atoms near the surface of SiO_2 particles link to silanolic OH groups. When a mixture is milled for 3 h, however, the Q_3 peak overlaps with Q_0. After 12 h, the Q_0 peak grows to be predominant, while Q_3 almost disappears. It is to be noted that the Q_0 peak in both MAS and CP/MAS NMR increase with milling time, with a preferential decrease in the Q_3 peak, while Q_4 is observed only by MAS NMR. From these observations, it seems safe to assume that the short-range ordering corresponding to calcium silicates is formed near a proton, since Q_0 is mainly attributed to hydrated calcium silicates.

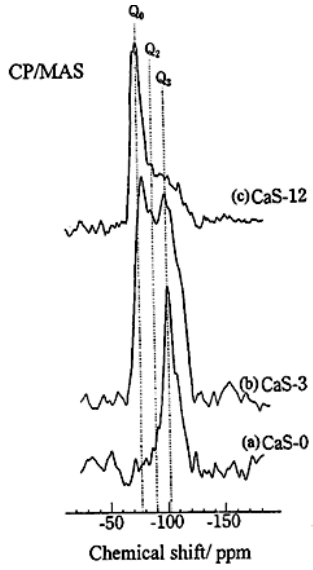

Figure 2. ^{29}Si CP/MAS NMR spectra of physically mixed (CaS-0) and milled samples (CaS-3,12), where -t indicates milling time in hours.[11] Reproduced by permission of Elsevier B.V

The bridging bond, Si-O-Ca, can also be formed via a radical recombination:

$$Ca(OH)_2: OH^- + OH^- \xrightarrow{\text{mechanical dehydration}} H_2 + O^- + O^-(Ca{-}O\cdot) \xrightarrow{\text{oxygen adsorption}} H_2 + O_3^- \quad (1)$$

These oxygen radicals can be formed even if mechanochemical dehydration takes place simultaneously. Meanwhile, the peroxy radicals can be formed by the following scheme:

$$SiO_2: \equiv Si{-}O{-}Si\equiv \xrightarrow{\text{mechanical activation}} \equiv Si{-}O\cdot + \equiv Si\cdot \xrightarrow{\text{oxygen adsorption}} \equiv Si{-}O\cdot \quad + \equiv Si{-}O{-}O\cdot(H). \quad (2)$$

Those bridging bonds like Si-O-Ca, mentioned above can be formed with many other complex oxide systems, by replacing Si with Ti, and Ca with Mg or Sr, and serve as nucleation points for the complex oxides.[12–14] These are also confirmed by simple simulation studies.[15,16] A model of the CaO/SiO_2 interface between two model clusters, $CaO_x^{(2x-2)-}$ and SiO_4^{4-} (Figure 3A), is adopted to calculate the electron density distribution of the cluster and the overlap population analysis. A self-consistent charge method,[33] which creates a Coulomb potential around a molecule by combining spherical atomic potentials, was used to obtain the Coulomb potential of the $Ca(OH)_6^{4-}$ and $SiO_4H_2^{2-}$ clusters. They were brought into contact, and the overlap population between the oxygen atom from $Ca(OH)_2$ and the hydrogen atom from silanol was examined. When an O atom from the SiO_4^{4-} cluster comes close to a Ca atom in the $CaO_x^{(2x-2)-}$ cluster, the population density, PD, between Ca and O increases with decreasing coordination number (CN) for Ca down to x = 3. This was combined with a simultaneous decrease in the PD between Si and O, as shown in Figure 3B. Decreasing in the coordination number is highly expected during the mechanochemical process, due to the introduction of oxygen vacancies.[34]

Molecular dynamic (MD) simulation was also used to elucidate the atomic rearrangement at the early stage of solid-state mechanochemical reaction at $Ca(OH)_2 - SiO_2$ interface in order to take the relaxation process into account. MD calculation was carried out by using a code MXDORTO.[35] Verlet algorithm was employed in order to calculate atomic motions.[36] A Ca–O bond, being fairly ionic, is represented by a Born–Mayer–Huggins (BMH) potential function, while for Si–O bond, we introduced an additional attractive term of the Morse potential to the BMH. Finally, to account for the O–H bonds, we added an extra three-body type potential. We derived inter-atomic forces from these potential energy functions within 1.5–2 nm around an atom by using a cell model of such a dimension.[36] Figure 4 represents time-resolved atomic configuration at the $Ca(OH)_2 - SiO_2$ interface. Between 8 and 10

ps, a hydrogen atom from SiO–H jumps into the surface of $Ca(OH)_2$ to attach to an oxygen atom of the group. Note that the principle described above is general so that it remains valid when Ca is replaced by Mg or Ba, and Si with Ti or Zr. Corresponding electroceramic materials are plenty, represented by $BaTiO_3$.

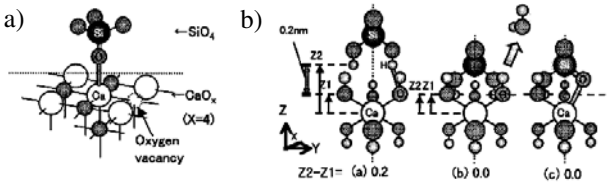

Figure 3. (A) $CaOx^{(2x-2)}$—SiO_4^{4-} cluster calculated for the CaO–Si-O_2, (B) $Ca(OH)_6^{4-}$–$SiO_4H_2^{2-}$ cluster calculated for the $Ca(OH)_2$–Si-O_2 interface: (a) the difference in the Z coordinates, Z2–Z1, is 0.2 nm, (b) Z2–Z1 is 0.0 nm. (c) $Ca(OH)_x^{(x-2)-}$–$SiO_4H_1^{3-}$ cluster after the dehydration at Z2–Z1 is 0.0. A Ca–O–Si bond is formed.[15] Reproduced by permission of American Chemical Society.

4. $BaBi_2Ta_2O_9$ (BBT) and $Ba(Mg_{1/3}Ta_{2/3})O_3$ (BMT)

Preparation of ferroelectric relaxors with simple or layered perovskite structures, BBT and BMT, was examined by a solid-state reaction via a soft-mechanochemical route.[37] For BBT, a stoichiometric mixture of $BaCO_3$, Bi_2O_3 and Ta_2O_5 was milled with in a vibratory mill and calcined for 1 h in air at temperatures between 850 and 1000 °C. As for BMT, $BaCO_3$ and $Mg(OH)_2$ were used as Ba and Mg sources, and either Ta_2O_5 or $Ta_2O_5 \cdot 3.8H_2O$ was used as a Ta source.

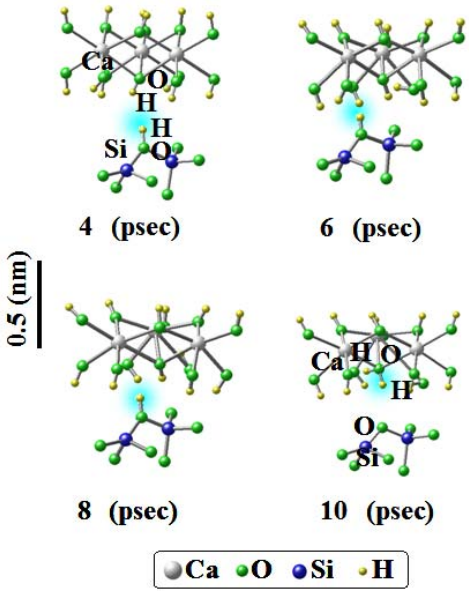

Figure 4. Configurations of $Ca(OH)_2$ –SiO_2 interface at 300 K, 0.1 MPa, representing a scheme of proton transfer from silanolic OH to O atom of $Ca(OH)_2$.[16] Reproduced by permission of Elsevier B.V

Fully crystallized, fine particulate BBT was obtained by calcining the mechanically activated starting mixture at 900 °C. The resultant particles are rather uniform with their average grain size as small as 400 nm. In the case of BMT, in contrast, a similar success was only reached by using hydrated sample, $Ta_2O_5 \cdot 3.8H_2O$, in place of anhydrous Ta_2O_5. As shown in Figure 5, the second phase, $BaTi_2O_4$, was almost disappeared, if not completely, by using mechanically activated mixture with $Ta_2O_5 \cdot 3.8H_2O$. The remarkable effect of milling is obvious, by comparing the calcined products starting from the intact mixture with $Ta_2O_5 \cdot 3.8H_2O$.

Oxygen 1s X-ray photoelectron spectrum (XPS) profiles are shown in Figure 6A for (a) Ta_2O_5-derived mixture, (b) sample (a) after milling for 3 h, (c) $Ta_2O_5 \cdot 3.8H_2O$ -derived mixture, (d) sample (c) after milling for 3 h, and (e) BMT obtained by calcining sample (d) at 900 °C, respectively. A second peak, appeared in curves (c) at the lower binding energy, ascribed to the hydrated water, disappeared after milling. We attributed this to the consumption of hydrated water due to the formation of bridging bonds, Ba–O–Ta and Mg–O–Ta across the boundary of dissimilar particle species.

The difference in the Ta4f XPS, shown in Figure 6B is particularly noteworthy. The profile of the curve (d), after milling the $Ta_2O_5 \cdot 3.8H_2O$-derived mixture is very close to that of well crystallized BMT (curve (e)), implying that the electronic state of Ta in the mechanically activated precursor was already very close to that of the final product.

Availability of pure-phase BBT and BMT is different, due to the difference in the easiness of bridging bond formation under mechanical stressing. BBT is a layered perovskite, in which $(Bi_2O_2)^{2+}$ and $(BaTa_2O_9)^{2-}$ layers align along c-axis, and the bonds between two dissimilar metals abridged by oxygen in BBT perovskite structure are mainly Ta–O–Ba. BMT, on the other hand, is a complex perovskite in which Ba occupies the A site and Mg and Ta, the B sites. In this case, Ta–O–Ba and Ta–O–Mg bonds coexist within the perovskite unit cell. In view of the acid–base reaction across the boundary of solid particles, Ta–O–Ba is easier to form than Ta–O–Mg, because of the higher basicity of Ba than Mg.

6. $KNbO_3$ (KN)

As we examined a soft-mechanochemical synthesis of $KNbO_3$, another lead-free piezoelectric perovskite, we first compared the two potassium sources, $KHCO_3$ and K_2CO_3, both starting from a mixture preliminarily vibromilled for 1 h.[38] No significant differences in the XRD profiles were observed between the starting potassium sources, but the particle size was significantly different,

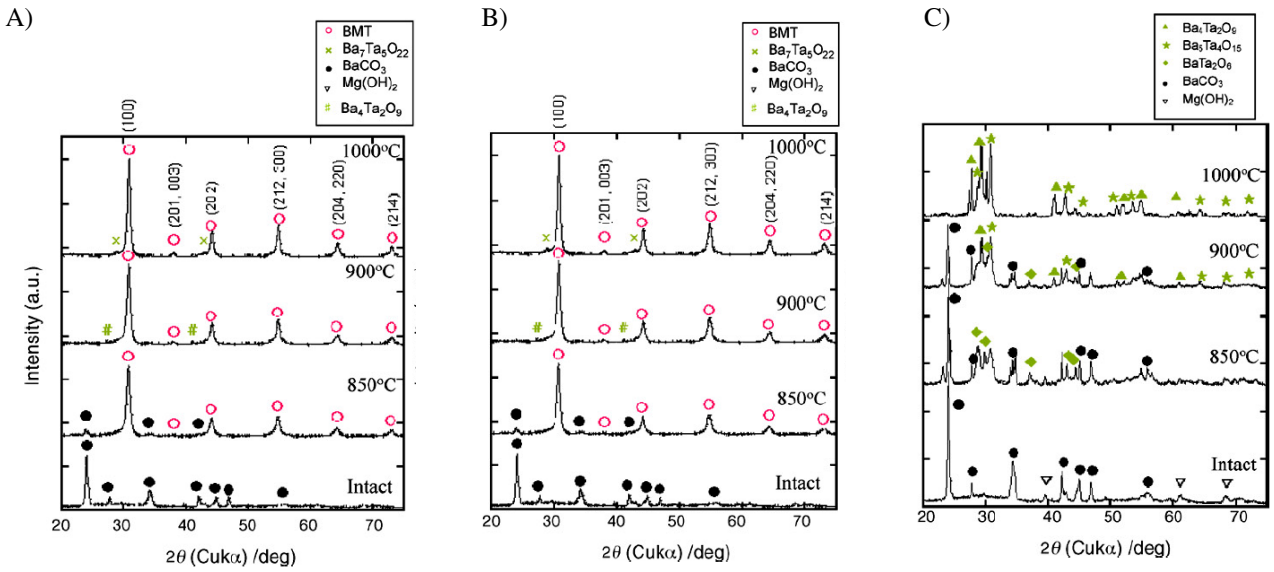

Figure 5. X-ray powder diffractograms for BMT calcined at varying temperatures derived from the mixtures containing (a) Ta_2O_5, milled for 3 h, (b) $Ta_2O_5 \cdot 3.8H_2O$ milled for 3 h and (c and b) $Ta_2O_5 \cdot 3.8H_2O$ without milling.[37] Reproduced by permission of Elsevier B.V

i.e. $KHCO_3$ brought about much smaller KN particles. When $KHNO_3$ agglomerates were preliminarily disintegrated, the product KN, became significantly smaller being close to that of the starting Nb_2O_5.

Mixing homogeneity of the starting mixtures or precursors on the particulate level was evaluated by electron probe microanalysis (EPMA). As shown in Figure 6, the mixture starting from $KHCO_3$ exhibits concentration area for potassium less than a few μm. By starting from

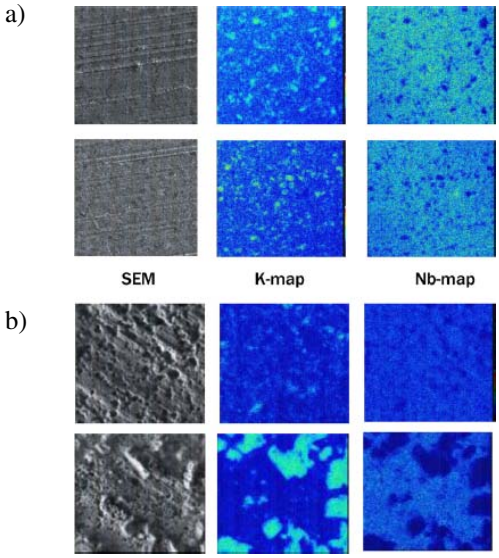

Figure 6. EPMA mapping of the vibro-milled mixture, starting from (a) $KHCO_3$ and (b) K_2CO_3. Two rows represent two different spots on the same sample. The entire width of each image is ca. 100 mm.[38] Reproduced by permission of Elsevier B.V.

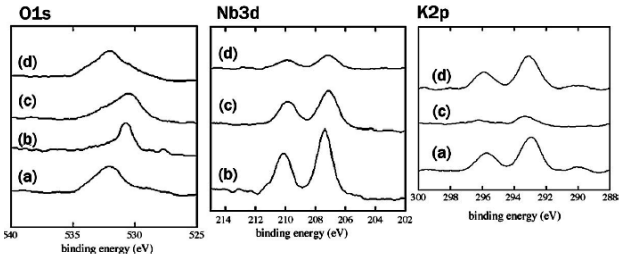

Figure 7. XPS profile of O 1s, Nb 3d and K 2p. Common keys: (a) $KHCO_3$, (b) Nb_2O_5, (c) $KHCO_3$ + Nb_2O_5 as hand mixed, (d) the mixture after vibro-milling for 3 h.[38] Reproduced by permission of Elsevier B.V.

K_2CO_3, we observe the high concentration area of potassium with its linear size more than 20 μm, as shown in Figure 8. The difference is ascribed to the severer agglomeration of K_2CO_3.

XPS profiles are shown in Figure 7 for the samples with $KHCO_3$. It is noteworthy that the Nb 3d signal weakened after vibro-milling, while the intensity of the K 2p signal increased, so that the effect of milling was quite opposite between Nb 3d and K 2p. In order to elucidate these changes, we observed the particle morphology under the scanning and transmission electron microscopes, equipped with energy dispersive X-ray spectroscopy (EDXS). A line scanning of the Nb–L, Nb–K and K–K signals clearly revealed the high concentrations of potassium in the near surface region and of niobium in the interior of the particle, as shown in Figure 8.

This explains the structure of the core–shell, i.e. Nb_2O_5-core enveloped by the $KHCO_3$ shell. The changes in the XPS signals by vibro-milling are quite compatible

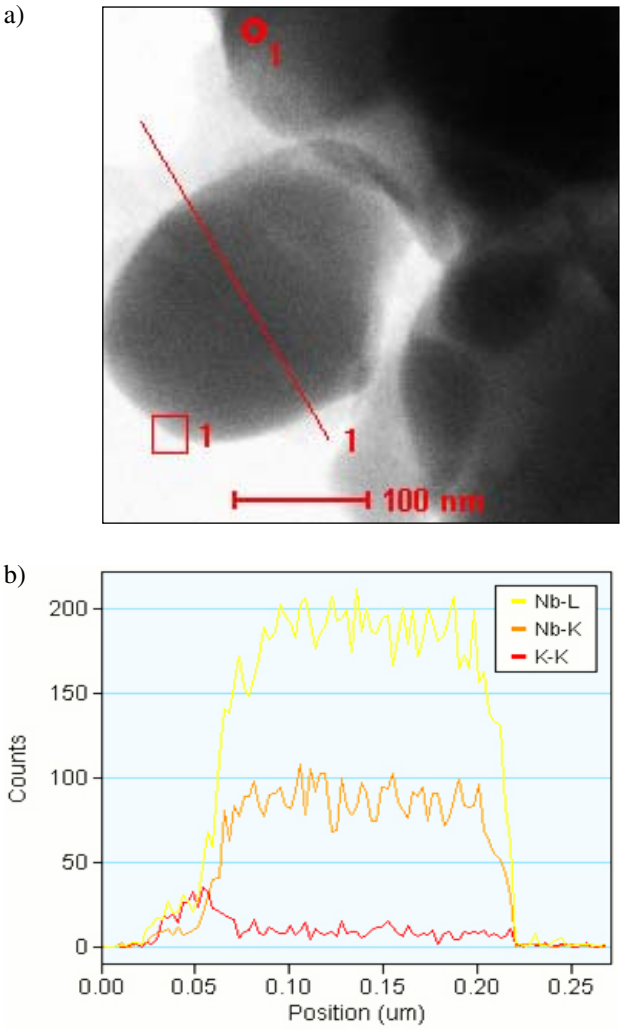

Figure 8. A TEM image of the precursor. B: Line profile of Nb and K by EDXS.[38] Reproduced by permission of Elsevier B.V.

with the present microscopy, coupled with the EDXS analysis. Before vibro-milling, the finer Nb_2O_5 particles simply cover the surface of $KHCO_3$. Therefore, the near surface Nb concentration is relatively higher than the average stoichiometry. During vibro-milling the mixture, $KHCO_3$ deformed plastically, surrounding the harder Nb_2O_5 particles and increasing the relative intensity of K 2p signals in the near surface region. Thus, the core–shell structure has most likely been formed under the shear stress exerted by a vibromill due to the substantial difference in their plasticity.

7. Summary

In the present short review, the author focused on the charm of formation of bridging bonds across the boundary between dissimilar particulate species by co-milling powder mixtures via a mechanochemical route. Mechanochemical synthesis of complex oxides is one of its direct manifestations. This was demonstrated in Section 2 with representative case studies. Combination of the mechanochemical process with a subsequent thermal process enables wider variation of the product complex oxides and their crystalline and granulometrical properties. The principle of these processes, coined as soft-mechanochemical processes was explained in Section 3. The mixture just after mechanical activation was defined as a precursor. Formation of potentially reactive precursors enables formation of the complex oxides at lower temperatures and hence smaller particle size with sufficiently high crystallinity. Subsequent 3 sections displayed case studies carried out in the author's own laboratory. The substances treated are all associated with the phase pure synthesis of lead-free ferroelectric materials, i.e. $BaBi_2Ta_2O_9$ (BBT), $Ba(Mg_{1/3}Ta_{2/3})O_3$ (BMT) and $KNbO_3$ (KN).

We know that most of the cutting-edge functional materials for better utilization of renewable energy and temporal energy storage are complex oxides, whose fabrication strategy needs to be more affordable and scalable. Since the method employed in this short review is based on the basic principle of the electronic and atomic transfer across the boundary among dissimilar solid species under mechanical stressing, it could be extended to many other systems beyond those introduced above.

8. Acknowledgements

The author sincerely thanks all the co-authors of his own works cited in the present review. It is also to be mentioned that the previous studies introduced here was extended to the later works carried out in the Laboratory of Electroceramics in Jozef Stefan Institute, initiated by the kind invitation of the late Professor Maija Kosec. Let the author express his sincere appreciation to her. Her discipline will be taken over by a number of her coworkers, including the author himself.

He also thanks the Alexander von Humboldt Foundation, by which his research stay in Braunschweig, Hannover and Karlsruhe was supported.

9. References

1. A. Marteel-Parrish, S. DeCarlo, D. Harlan, J. Martin, H. Sheridan, *Green Chem. Let. Rev*. **2008**, *1*, 231–239.
2. N. Rakov, R. B. Guimarães, W. Lozano B., G. S. Maciel, *J. Appl. Phys*. **2008**, *114*, 043517.
3. P. Abhilash, D. Thomas, K. P. Surendran, and M. T. Sebastian, *J. Am. Ceram. Soc*. **2013**, *96*, 1533–1537.
4. K. He, R. Y. Hong, W. G. Feng, D. Badami, P*owder Technol*. **2013**, *239*, 518–524
5. K. G. S. Pannu, T. Pannu, T. Fürstenhaupt, V. Thangadurai, Solid State Ionics, **2013**, *232*, 106–111.

6. V. Sepelak, A. Duvel, M. Wilkening, K.-D. Becker, P. Heitjans, *Chem. Soc. Rev*. **2013**, *42*, 7507–7520.
7. E. Avvakumov, M. Senna, N. Kosova, "Soft Mechanochemical Synthesis," Kluwer Acad. Pub., New York, **2001**, pp. 145–66.
8. M. Senna, *Solid State Ionics*, **1993**, *63–65*. 3–9.
9. J. F. Liao, M. Senna, *Solid State Ionics*, **1993**, *66*, 313–319.
10. T. Watanabe, T. Isobe, M. Senna, *J. Solid State Chem*. **1996**, *122*, 291–296.
11. T. Watanabe, T. Isobe, M. Senna, *J. Solid State Chem*. **1997**, *130*, 284–289.
12. M. Senna, *Chem. Rev*. **1998**, *123*, 263–84.
13. M. Senna, *Int. J. Inorg. Mater*. **2001**, *3* 509–14.
14. M. Senna, *Mater. Sci. Eng. A*, **2001**, A304–306, 39–44.
15. Y, Fujiwara, T. Isobe, M. Senna, J. Tanaka, *J. Phys. Chem. A*, **1999**, *103*, 9842–9846.
16. M. Senna, Y. Fujiwara, T. Isobe, and J. Tanaka, *Solid State Ionics*, **2001**, *141–142*, 31–38.
17. R. Yanagawa, C. Ando, H. Chazono, H. Kishi, M. Senna, *J. Am. Ceram. Soc*. **2007**, *90*, 809–814.
18. K. Oguchi, C. Ando, H. Chazono, H. Kish, M. Senna, J. Phys. IV France, **2005**, *128*, 33–39.
19. C. Ando, T. Suzuki, Y. Mizuno, H. Kishi, S. Nakayama, M. Senna, *J. Mater. Sci*. **2008**, 43, 6182–6192.
20. T. Rojac, M. Kosec, B. Malic, J. Holc, *J. Eur. Ceram. Soc*. **2006**, *26,* 3711–3716.
21. T. Rojac, Ž. Trtnik, M. Kosec, *Solid State Ionics*, **2011**, *190*, 1–7.
22. T. Rojac, A. BenWan, M. Kosec, *J. Am. Ceram. Soc*. **2010**, *93*, 1619–1625.
23. T. Rojac, M. Kosec, P. Segedin, B. MaliW, J. Holc, *Solid State Ionics*, **2006**, *177*, 2987–95.
24. B. D. Stojanovic, A.Z. Simoes, C. O. Paiva-Santos, C. Jovalekic, V. V. Mitic, J. A. Varela, *J. Eur. Ceram. Soc*. **2005**, *25*, 1985–1989.
25. Z. Ž. Lazarević, B. D. Stojanović, M. J. Romčević, N. Ž. Romčević, *Sci. Sinter*. **2009**, *41*, 19–26.
26. Z. Z. Lazarevi, N. Z. Romcevi, J. D. Bobic, M. J. Romcevic, Z. Dohcevic-Mitrovic, B. D. Stojanovic, *J. Alloy Compound*, **2009**, *486*, 848–852.
27. V. Sepelak, M. Myndyk, M. Fabian, K. L. Da Silva, A. Feldhoff, D. Menzel, M. Ghafari, H. Hahn, P. Heitjans, K.-D. Becker, *Chem. Commun*. **2012**, 48, 11121–11123.
28. K. L. Da Silva, D. Menzel, A. Feldhoff, C. Kübel, M. Bruns, A. Paesano Jr., A. Düvel, M. Wilkening, M. Ghafari, H. Hahn, F. J. Litterst, P. Heitjans, K.- D. Becker, V. Sepelak, *J. Phys. Chem. C*, **2011**, *115*, 7209–7217.
29. A. Sen, T. Kar, S. K. Pradhan, *J. Alloys Compd*. **2013**, *557*,47–52.
30. T. F. Marinca, I. Chicinas, O. Isnard, *Ceram. Int*. **2013**, *39*, 4179–4186.
31. A. M. Bolarín-Miró, F. Sánchez-De Jesús, C. A. Cortés-Escobedo, R. Valenzuela, S. Ammar, *J. Alloys Compd*. **2014**, *586*, 590–594.
32. M. A. Lopez-Heredia, M. Bohner, W. Zhou, A. J. A. Winnubst, J. G. C. Wolke, J. A. Jansen, *J. Biomrf. Mater. Res. B. Appl. Biomater*, **2011**, *98B*. 68–79.
33. A. Rosen, D. E. Ellis, H. Adachi, F. W. Averill, *J. Chem. Phys*. **1976**, *65*, 3629–3634.
34. M. Senna, V. Sepelak, J. Shi, B. Bauer, A. Feldhoff, V. Laporte, K.-D. Becker, *J. Solid State Chem*. **2012**, *187*, 51–57.
35. K. Kawamura, MXDORTO, Japan Chemistry Program Exchange, 1998.
36. J. Verlet, Phys. Rev. **1967**, *159*, 98.–103.
37. M. Senna, T. Kinoshita, Y. Abe, H. Kishi, C. Ando, Y. Doshida, B. Stojanovic, *J. Eur. Ceram. Soc*. **2007**, *27*, 4301–4306.
38. T. Kinoshita, M. Senna, Y. Doshida, H. Kishi, *Ceram. Intern*. **2012**, *38*, 1897–1904.

Povzetek

V preglednem članku so obravnavani procesi v trdnem stanju, ki vodijo do fazno čistih in dobro kristaliziranih kompleksnih oksidov elektronske keramike. Povečanje reaktivnosti in ohranjanje stehiometrije reakcijskih mešanic ali prekurzorjev sta splošnega pomena. Pri mehanokemijski aktivaciji sta izpostavljena kontaminacija reagentov in racionalizacija procesov. Po kratkem pregledu mehanokemijskih procesov, ki omogočajo direktno sintezo kompleksnih oksidov, so v članku obravnavani procesi med mehanokemijsko aktiviranimi prekurzorji, ki potekajo v trdnem stanju. Opisanih je nekaj primerov sinteze kompleksnih oksidov iz literature, vključene so tudi avtorjeve raziskave $BaBi_2Ta_2O_9$ (BBT), $Ba(Mg_{1/3}Ta_{2/3})O_3$ (BMT) in $KNbO_3$ (KN). Večinoma gre za feroelektrične materiale, nekaj je tudi magnetnih materialov, ki vsebujejo železo.